

Radio bounds on the mixed dark matter scenarios of primordial black holes and WIMPs

Kenji Kadota^{1,2} and Hiroyuki Tashiro³

¹School of Fundamental Physics and Mathematical Sciences, Hangzhou Institute for Advanced Study, University of Chinese Academy of Sciences (HIAS-UCAS), Hangzhou 310024, China

²International Centre for Theoretical Physics Asia-Pacific (ICTP-AP), Beijing/Hangzhou, China

³Department of Physics and Astrophysics, Nagoya University, Nagoya 464-8602, Japan

We study the synchrotron radio emission in the mixed dark matter scenarios consisting of the primordial black holes (PBHs) and the self-annihilating WIMPs (weakly interacting massive particles). The WIMPs can form the ultracompact minihalos around PBHs and the annihilation enhancement from these dense halos can lead to the efficient synchrotron radiation at the radio frequency in the presence of galactic magnetic fields. The upper bound of PBH fraction with respect to the total dark matter abundance is of order $10^{-8} \sim 10^{-5}$ depending on the electroweak scale WIMP mass ($m_\chi = 10 \sim 1000$ GeV) and the WIMP annihilation channel (e.g. a hadronic $\chi\chi \rightarrow b\bar{b}$ or a leptonic $\chi\chi \rightarrow e^+e^-$ channel). The PBH contribution to the total dark matter abundance is hence negligible when the other component of dark matter is composed of the conventional electroweak scale WIMPs.

I. INTRODUCTION

The nature of dark matter (DM) still remains elusive despite the convincing evidence for its existence from the astrophysical observations. Commonly discussed DM candidates include the weakly interacting massive particles (WIMPs) motivated from supersymmetry and the axion or more generally axion like particles motivated from pseudo-Nambu-Goldstone bosons arising from the spontaneous symmetry breaking in the early Universe [1–8]. Moreover the DM do not need to be fundamental particles and the detection of gravitational waves [9–11] revived the interests in the primordial black hole (PBH) DM. While the parameter space for the PBH to account for the whole DM of the Universe is being narrowed due to the observation data such as those from the gravitational lensing, PBHs being a partial DM component still remains an intriguing possibility [12–14]. In particular we consider the scenarios where the DM is composed of PBHs and WIMPs and study the radio observation bounds on the allowed PBH abundance. Most of the previous literature studying such PBH-WIMP mixed DM scenarios focused on the gamma ray and more recently on the CMB and 21cm bounds [15–30]. While the synchrotron radio emission bounds on the WIMP annihilation have been actively discussed in the literature, little attention has been given to the synchrotron radiation in the context of PBH-WIMP mixed DM scenarios which is the focus of our paper [31–38]. The radio observations can give complimentary to and in some cases tighter bounds on the DM properties than those from gamma rays [34–38]. There also have been the works discussing the radio signals from the evaporation of PBHs via Hawking radiation for which the typical PBH mass range explored is of order $M_{PBH} \sim 10^{15} - 10^{17}$ g [39–43]. Our radio signal study explores the totally different PBH mass range of order a solar mass ($1M_\odot \sim 2 \times 10^{33}$ g).

Because different wavelength observations can have different systematics and sensitivities to the potential signals, it would be of great interest to check if the multi-wavelength observations support or disprove each other’s analysis for the further scrutiny of potential DM signals. The DM annihilation can produce the particles covering a wide range of energy spectra. In particular, we are interested in the synchrotron radio emission from the energetic electrons/positrons in the presence of the galactic magnetic fields.

We study the synchrotron radio emission from the WIMP halos around PBHs. The WIMPs can accrete to a PBH to form the ultracompact minihalo (UCMH) around it. The UCMH can possess a steep density profile and the WIMP annihilation which is proportional to the WIMP density squared is expected to be enhanced. Among the particles produced from such enhanced WIMP annihilation, the relativistic electrons (or positrons) (e^\pm can be the WIMP annihilation final state or more commonly can come from the hadronization and cascade decays of final states) are of particular interest in our study because their synchrotron radiation lies in the observable radio frequency. The synchrotron radiation can be indeed the main source of energy loss for electrons when they have the energy of order a few GeV and above typical for the weak scale mass WIMPs. This is especially the case in the Galactic center where the magnetic field can be bigger than that corresponding to the equivalent CMB energy density ($B \gtrsim 3.25(1+z)^2 \mu G$, $z = 0$ for our study), so that the synchrotron radiation overcomes another main source of energy loss due to inverse Compton scattering with the ambient CMB photons. We also mention that the electron energy loss due to the synchrotron radiation is proportional to the square of electron energy, as well as the magnetic field squared, and hence is suppressed for the lighter WIMP mass. For instance, the energy loss due to Coulomb interactions with thermal plasma can dominate those due to synchrotron radiation and inverse Compton scattering for the sub-GeV electron

energy. We focus on the typical weak scale WIMP mass range above GeV scale in this paper. Another reason for our restricting our discussions to the above GeV WIMP mass as well as the solar mass range for the PBH mass is to assume that the kinetic energy of WIMPs is negligible compared with its potential energy under the influence of PBH's gravity. The WIMP halo formation around the PBH can well be disturbed by WIMP kinetic energy leading to a less dense profile. Consequently the WIMP annihilation signals become smaller and the bounds on the allowed PBH DM fraction are expected to be significantly weakened when the kinetic energy is not negligible [18, 21, 44]. For the sub-GeV WIMP mass, on the other hand, the other bounds different from considering the UCMHs around PBHs can give tight bounds such as those due to the enhanced isocurvature perturbations from the Poisson fluctuations in PBH distributions [45–53]. The kinetic energy of WIMP is heavily model dependent [54–61] and we leave the study for the scenarios with non-negligible WIMP kinetic energy for future work.

The quantitative comparison with the previous relevant works is in order. The previous papers studying the gamma ray bounds on the PBH-WIMP mixed DM scenarios gave the bounds from the Milky Galaxy of order $f_{PBH} \lesssim \mathcal{O}(10^{-9}) \sim \mathcal{O}(10^{-7})$ for $m_\chi \sim 10^1 - 10^3$ GeV when the primary annihilation channel is $\chi\chi \rightarrow b\bar{b}$ [15–29]. $f_{PBH} \equiv \Omega_{PBH}/\Omega_{DM}$ is the PBH abundance fraction with respect to the total dark matter abundance and the total dark matter consists of PBHs and WIMPs ($\Omega_{DM} = \Omega_{PBH} + \Omega_\chi$). There have been recent studies discussing the CMB and 21cm bounds which also demonstrated the bounds comparable to the gamma rays [28, 30]. Our radio bounds lead to the upper bounds $f_{PBH} \lesssim \mathcal{O}(10^{-8}) \sim \mathcal{O}(10^{-7})$ for $m_\chi \sim 10^1 - 10^3$ GeV when $\chi\chi \rightarrow b\bar{b}$, and hence support the claim of the other frequency observations that the PBH DM and WIMP DM cannot coexist.

Section II outlines our model setup where we illustrate the WIMP halo possessing the steep density profile formed around a PBH. Due to the large WIMP density around a PBH, one can expect the large enhancement in the WIMP annihilation which is proportional to the WIMP density squared. Section III then presents the expected radio signals due to the synchrotron radiation from the energetic e^\pm arising from the WIMP annihilation, and compare them with the observation data to put the bounds on the allowed PBH abundance. Sec IV is devoted to the discussion/conclusion. Throughout the paper, our discussions assume $f_{PBH} \ll 1$ unless stated otherwise (equivalently $1 - f_{PBH} \approx 1$ and this assumption is justified in our quantitative analysis in Section III).

II. SETUP

We first outline the UCMHs (ultracompact minihalos) around primordial black holes which can possess the steep WIMP density profile $\rho(r) \propto r^{-9/4}$ [16, 18–20, 44, 62]. The WIMP particles can accrete to PBHs when the PBHs are formed in the radiation dominated epoch, and we aim to study the effects of the resultant enhanced WIMP annihilation on the radio signals. The WIMP density profile can be estimated via the spherical collapse model where the turn around radius is numerically estimated as [19]

$$r_{ta} \approx (R_S t_{ta}^2)^{1/3} \quad (1)$$

which represents the scale at which a WIMP particle decouples from the background Hubble flow under the gravitational influence of a PBH. $R_S = 2GM_{PBH}$ is the Schwarzschild radius, M_{PBH} is the PBH mass, and t_{ta} is the turn around time when a WIMP particle stops moving away from a PBH and starts falling towards it at r_{ta} . Assuming each mass shell density matches the background density at the turn around, the WIMP halo density profile during the radiation dominated epoch can be estimated as

$$\rho_{sp}(r) \approx \frac{\rho_{eq}}{2} \left(\frac{t_{ta}}{t_{eq}} \right)^{-3/2} \approx \left(\frac{\rho_{eq}}{2} \right) t_{eq}^{3/2} (2GM_{PBH})^{3/4} r^{-9/4}. \quad (2)$$

Such a steep profile $\rho_{sp}(r) \propto r^{-9/4}$ (possessing a "spike" in contrast to a more conventional "cusp" such as in the NFW profile [63]) was also verified in the numerical simulations [19, 62]. While the UCMH around a PBH can grow during the matter domination epoch according to the secondary infall mechanism, we conservatively consider the annihilation only from the region inside the turn around radius at the matter radiation equality $r_{ta}(z_{eq}) \sim 0.04(M_{PBH}/M_\odot)^{1/3}$ pc. It was verified numerically that such a steep profile is maintained even if the outer part of the halo follows the conventional less steep profile (e.g. NFW profile) [19, 62]. The spike profile $\rho \propto r^{-9/4}$ makes the WIMP annihilation so efficient around the center of a halo, so that the density can saturate when the WIMP annihilation time scale becomes comparable to the age of the WIMP halo. The density of such an annihilation plateau in the core region can be taken account of as

$$\rho_{max}(t) \approx \frac{m_\chi}{\langle \sigma v \rangle (t - t_i)} \quad (3)$$

where m_χ is the WIMP mass, $\langle\sigma v\rangle$ is the thermally averaged WIMP annihilation cross section, t_i is the formation time of UCMH (in our quantitative calculations for the signals from the Milky Way Galaxy, $t \gg t_i$ is the age of the Universe and $t - t_i \approx t$). The UCMH density profile hence reads [16, 18–21, 28, 30, 44, 64–68]

$$\rho_{UCMH}(r) = \begin{cases} 0 & \text{for } r < 4GM_{PBH} \\ \frac{\rho_{sp}(r)\rho_{max}(r)}{\rho_{sp}(r)+\rho_{max}(r)} & \text{for } 4GM_{PBH} \leq r < r_{ta}(t_{eq}). \end{cases} \quad (4)$$

A WIMP particle is captured by a black hole for $r < 2R_S = 4GM_{PBH}$ setting the inner radius of a halo [69, 70]. The second line comes from integrating $\dot{n}_\chi = -n_\chi^2\langle\sigma v\rangle$ with $\rho_\chi = n_\chi m_\chi$. The UCMH profiles for a few representative parameter sets are shown in Fig. 1. There is a transition from the inner spike region ρ_{max} forming a core with a flat amplitude to the outer spike region $\rho_{sp} \propto r^{-9/4}$ at a radius $r_{core} \propto m_\chi^{-4/9} M_{PBH}^{1/3}$ characterized by $\rho_{max}(r_{core}) = \rho_{sp}(r_{core})$. The annihilation plateau amplitude $\rho = m_\chi\langle\sigma v\rangle^{-1}t^{-1}$ increases for a bigger m_χ because of the smaller WIMP number density to annihilate and decreases for a bigger annihilation cross section and at a later time because more WIMP particles annihilate. The majority of annihilation products come from the region $r \sim r_{core}$ and considering the profile at a larger radius $r \gtrsim r_{ta}(z_{eq})$ does not significantly affect our discussions because of the small density [18–22, 28, 30, 71]. The annihilation signal contributions from the regions well inside r_{core} does not significantly affect our discussions either because of the small volume despite the large WIMP density. Our goal is to estimate the radio signals from these UCMHs around PBHs in our Milky Way Galaxy.

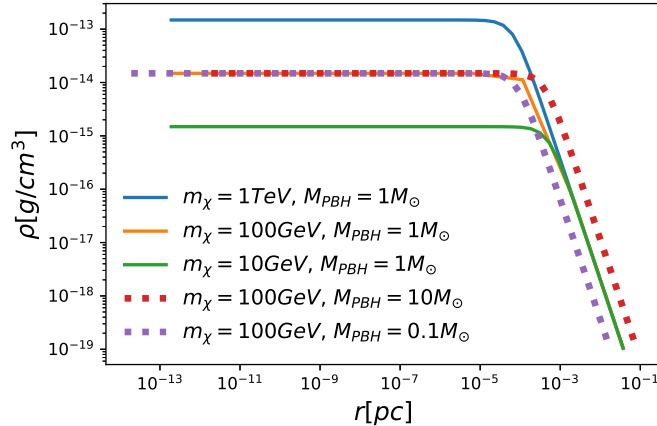


FIG. 1: The UCMH density profile around a PBH as a function of the radius. The WIMP mass m_χ and the PBH mass M_{PBH} are varied. Each curve covers the radius from $r_{min} = 4GM_{PBH}$ to the turn around radius at the matter radiation equality $r_{ta}(z_{eq})$.

III. RESULTS

We aim to obtain the radio bounds on the allowed PBH fraction in the PBH-WIMP mixed DM scenarios. The energetic e^\pm originating from the WIMP annihilation can emit synchrotron radiation in the radio frequency and one can expect the enhancement of such radio signals due to the enhanced WIMP density around PBHs.

It is customary to use the brightness temperature $T_B[K]$ in the radio observations (k_B is the Boltzmann constant)

$$T_B = \frac{c^2}{2\nu^2 k_B} I_\nu \quad (5)$$

which is related, by the Rayleigh-Jeans law, to the specific intensity $I_\nu[\text{erg cm}^{-2}\text{s}^{-1}\text{Hz}^{-1}\text{sr}^{-1}]$ (the flux density per solid angle per unit frequency). For the signal from a direction (l, b) (longitude l and latitude b in the galactic coordinate), the specific intensity is obtained by integrating the emissivity j_{syn} along the line of sight

$$I_\nu(l, b) = \int_{LOS} ds \frac{j_{syn}(\nu, r(s, l, b))}{4\pi} \quad (6)$$

with the emissivity at a frequency ν

$$j_{syn}(\nu, r) = 2 \int_{m_e}^{M_{DM}} dE \frac{dn_e(E, r)}{dE} P_{syn}(\nu, E, r) \quad (7)$$

where P_{syn} is the synchrotron power emitted by an electron at a frequency ν averaged over all directions [72]. A factor 2 takes account of the contributions from both electrons and positrons. For a given point with the distance s along the line of sight, the distance r from the Galactic center can be given in terms of the galactic coordinate $r^2(s, l, b) = s^2 - 2sr_{\odot} \cos b \cos l + r_{\odot}^2$ (where $r_{\odot} = 8.33$ kpc is the Sun's distance from the Galactic center). To estimate the radio signals of our interest, we need to know the electron/positron energy spectrum originating from the WIMP annihilation. Those energetic electrons/positrons diffuse through the galactic medium while losing energy due to the processes such as the synchrotron radiation and the inverse Compton scattering. The final electron number density per unit energy $dn_e(E, r)/dE$ can be obtained by solving the diffusion-loss equation [72–74]

$$\frac{\partial}{\partial t} \frac{dn_e(E, r)}{dE} = \nabla \cdot \left[K(E, r) \nabla \frac{dn_e(E, r)}{dE} \right] + \frac{\partial}{\partial E} \left[b(E, r) \frac{dn_e(E, r)}{dE} \right] + Q(E, r) \quad (8)$$

where E denotes the energy of electrons. The source term in our PBH-WIMP mixed DM scenario is

$$Q(E, r) = n_{PBH} \Gamma_{PBH}^f \frac{dN_e^f(E, r)}{dE} \quad (9)$$

$$n_{PBH} = \frac{f_{PBH} \rho_{Gal}}{M_{PBH}}, \quad \Gamma_{PBH}^f = \frac{1}{2m_{\chi}^2} \int dR 4\pi R^2 \rho_{UCMH}^2 \langle \sigma v \rangle_f. \quad (10)$$

We for concreteness assume Majorana particles for WIMPs. K, b represent respectively the diffusion coefficient and energy loss coefficient [34, 36, 72, 75–80]. Morphologically the WIMP annihilation signals from the unresolved UCMHs around PBHs can be interpreted as the signals from the ‘decaying’ PBHs dressed by WIMPs. Hence the source term resembles that for a decaying DM scenario with the decay rate Γ . dN_e^f/dE represents the electron energy distribution per one WIMP annihilation with a given final state channel f (we will later consider $\chi\chi \rightarrow b\bar{b}$ channel and $\chi\chi \rightarrow e^+e^-$ channel for illustration purposes). We assume the PBH number density distribution $n_{PBH}(r)$ follows the underlying Galaxy density profile $\rho_{Gal}(r)$ modeled by the NFW profile. In estimating the synchrotron radio emission from the dressed PBHs, we simply treat the UCMHs as unresolved point-like objects which are embedded in the Milky Way Galaxy’s magnetic fields¹. The tidal disruptions of substructures inside a host halo are still under active debate. While the outskirts of the compact halos can be tidally stripped away, the dense core parts may well survive where the dominant DM annihilation signals come from [82–90]. We simply assume the core of an UCMH is unaffected by tidal forces and leave the further studies including the effects of tidal disruptions and the detailed UCMH spatial distributions for future work. We accordingly consider the annihilation only from the core region of UCMH $r \leq r_{ta}(z_{eq}) \sim 0.04(M_{PBH}/M_{\odot})^{1/3}$ pc in calculating Γ_{PBH}^f . One can obtain the steady state equilibrium solution for dn_e/dE by the Green’s function method [73, 75, 77, 79, 91] and we use the PPC4DM package for our numerical calculations [79, 91]. To estimate the signals, one needs to specify the cosmic ray’s diffusion model and our choices are described in the following. In treating the charged particle propagation, we adopt the conventional parameterization of the diffusion coefficient $K = K_0(E/GeV)^{\delta}$ which is position-independent but depends on the energy. Those diffusion coefficients can be determined from the cosmic ray abundance measurements such as those of boron-to-carbon ratio and the conventional propagation parameter sets adopted in our analysis are $(\delta, K_0[\text{kpc}^2/\text{Myr}], L[\text{kpc}]) = (0.55, 0.00595, 1), (0.70, 0.0112, 4), (0.46, 0.0765, 15)$, often referred to respectively as MIN, MED, MAX models (the primary anti-proton fluxes due to the DM annihilation in the Milky Way halo are minimal, median or maximal at the solar position) [74, 79, 91–93]. The cylindrical diffusion zone has the height $2L$ and radius 20 kpc. The MED propagation parameters are commonly used in the literature and we present our results using the MED model in this section. Using MIN and MAX models do not affect our discussions as demonstrated in the discussion section. $b(E) = b_{syn} + b_{ICS} + b_{Coul} + b_{brem}$ includes the effects of energy loss due to synchrotron radiation, inverse Compton scattering, Coulomb interaction and bremsstrahlung [34, 36, 72, 75–80]. We modeled the energy loss rate $b(E)$ as in Ref. [79]. We note that, for the parameter range of our interest (the typical energy scale of e^{\pm} is \gtrsim GeV), the energy loss is dominated by the synchrotron radiation and the inverse Compton scattering. The estimation of energy loss

¹ The length scale for the e^{\pm} to lose a half of its energy and also its diffusion length scale are larger than the scales relevant for the UCMHs [35, 81].

due to the synchrotron radiation $b_{syn}(E) \propto E^2 B^2$ requires us to specify the magnetic field profile B for which we adopt the following conventional profile [91, 94]

$$B(r, z) = B_0 \exp[-(r - r_\odot)/r_B - |z|/z_B] \quad (11)$$

The common choices for the magnetic field configuration parameters are $B_0 = 4.78 \mu\text{G}$, $r_B = 10 \text{ kpc}$, $z_B = 2 \text{ kpc}$ referred to as the model MF1 and $(B_0[\mu\text{G}], r_B [\text{kpc}], z_B [\text{kpc}]) = (5.1, 8.5, 1)$ and $(9.5, 30, 4)$ respectively referred to as the MF2 and MF3 models. MF1 is the configuration similar to that used in GALPROP code [94], MF2 is based on Ref [95] which has a bigger spatial gradient with a higher magnitude at the Galactic center and MF3 has a much bigger magnitude at the Earth location and the magnetic field region extends much further than the other models [96]. The effects due to the variation in the magnetic field parameters are degenerate with those due to the variation of the aforementioned propagation parameters. In fact, we found the difference in the synchrotron radiation signals among these three magnetic field parameter sets is much smaller than that among aforementioned MIN/MED/MAX models. We therefore simply present our findings using the MF1 model for the magnetic field configuration. The estimation of energy loss due to the inverse Compton scattering requires the photon distributions which e^\pm scatters with, and, following Ref. [91], we adopt the blackbody spectrum for the CMB photons and the map from GALPROP for infrared light and star light [97]. We note, at radio frequencies, the energy loss is dominated by the synchrotron radiation in the Galactic center for the parameter range of our interest due to the large magnetic field where the dominant signals come from (in the presence of the reasonably strong magnetic field bigger than that corresponding to the equivalent CMB energy density $B \gtrsim 3.25(1+z)^2 \mu\text{G}$ (the redshift $z = 0$ in our calculations)).

Using these model parameters, we can make predictions on the expected signals in our PBH-WIMP mixed DM scenarios as shown in Fig. 2 along with the observed radio emission data. The figures are plotted as a function of the galactic latitude b along the galactic longitude $l = 0$. The chosen parameter sets are $m_\chi = 100 \text{ GeV}$, $\langle\sigma v\rangle = 3 \times 10^{-26} \text{ cm}^3/\text{s}$, $M_{PBH} = 1M_\odot$ and the primary annihilation channel $\chi\chi \rightarrow b\bar{b}$. The MED propagation model, MF1 magnetic field model and the NFW density profile are used for the Milky Way Galaxy. The spherical symmetry is assumed in the signal calculations. The signals and foregrounds are bigger towards the Galactic center because of the bigger magnetic field and DM density. While we chose the data at 45 MHz and 408 MHz because of the data availability, some further comments on our choice of frequencies are in order. For the WIMP mass below 10 TeV, the synchrotron radiation signals in the Galaxy typically peak at below tens of GHz with a magnetic field of order μG . In choosing the observation data to compare with the signals, we also prefer those below a GHz to ensure that the measured temperature is dominated by the synchrotron radiation to avoid being plagued by the other contributions such as the free-free, thermal dust and CMB radiation. We accordingly choose the observation maps with a large sky coverage at 45 MHz and 408 MHz from Ref. [98–101] (for which the data are available for the whole sky). The angular resolution of 45 MHz map is worse than that of 408 MHz map (the survey angular resolutions are respectively 5 degrees and 0.85 degrees) and the flux in the Galactic central region in our plots is more smoothed out in the former. These maps suffice for our purpose to put the bound on the PBH fraction. We constrain f_{PBH} by demanding that the expected DM signals should not exceed the observed data with 3σ , $T_{DM} < T_{data} + 3\sigma_{data}$ at all latitudes along the longitude $l = 0$. The map at 45 MHz was obtained by combining the southern and northern surveys and the root mean square temperature noise is 300 K/2300 K for the southern/northern data and that at 408 MHz is of order one Kelvin. The error bars of the radio data used in our analysis hence are an order of magnitude smaller than the observed temperature and do not give appreciable impacts on our bounds, especially in comparison to the systematic uncertainties in theoretical cosmic ray propagation modeling [31, 79, 100]. We can see from these figures that the bounds mainly come from the central region of the sky. For the region outside the central Galactic region where the magnetic field is smaller, the synchrotron signal typically peaks at a frequency below one MHz and the majority of signals can lie below the observable frequencies accessible by the radio telescopes. The tight bounds hence can come from the central region of our Galaxy even though the synchrotron radiation can cover a wide range of frequency beyond its peak frequency. We will show in the discussion section that the bound would not change by more than an order of magnitude even if we take account of the large systematic uncertainties such as those in the propagation models and the magnetic field profile. The left panel of Fig. 3 shows the consequent upper bounds on f_{PBH} for $\chi\chi \rightarrow b\bar{b}$ illustrated in Fig. 2. We can see that the PBH DM abundance is negligible ($f_{PBH} \ll 1$) when the WIMP DM is the rest of DM of our Universe. One can do the same exercises for the leptonic channel too and the bounds for the $\chi\chi \rightarrow e^+e^-$ annihilation scenario are also shown in Fig. 3. Note our bounds on f_{PBH} is insensitive to the values of M_{PBH} , which is also the case for the gamma ray bounds on f_{PBH} [15–29]. This is simply because of the cancellation of the M_{PBH} dependence between $\Gamma_{PBH} \propto M_{PBH}$ and $n_{PBH} \propto M_{PBH}^{-1}$. The dependence of the upper bounds of f_{PBH} on M_{PBH} however shows up, for instance, when the annihilation cross section is velocity dependent [71] or when the kinetic energy of WIMP is not negligible preventing the steep profile around a PBH (which can be the case for $M_{PBH} \lesssim 10^{-3}M_\odot$ if $m_\chi \lesssim 10 \text{ GeV}$ [18–21, 44, 47]). The non-trivial relative ordering of the bounds illustrated in this figure stems from the non-trivial frequency dependence of the signals and the observational data used. The relative comparison of the signals for the $b\bar{b}$ and e^+e^- annihilation channels as a function of the frequency

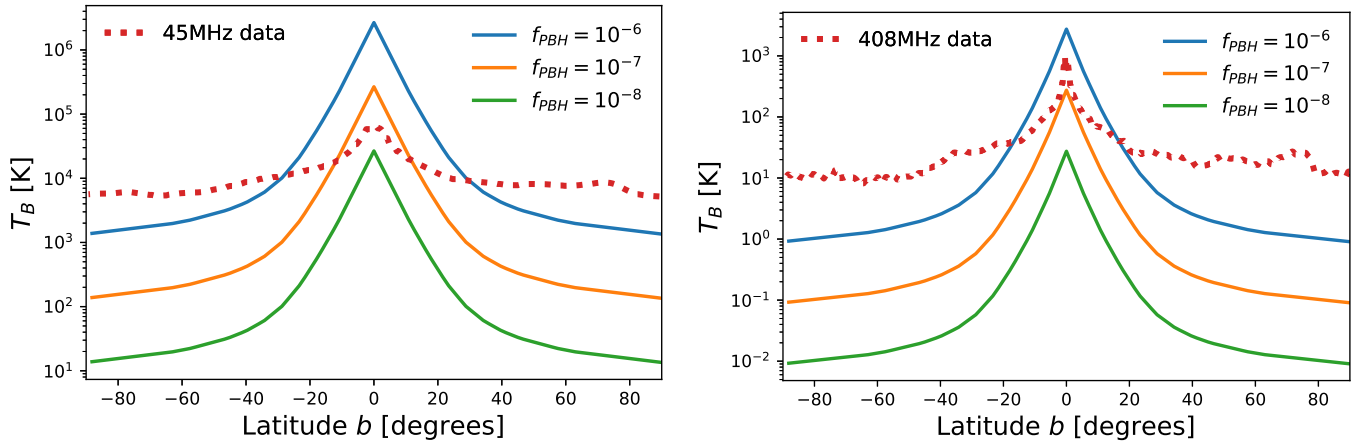


FIG. 2: The brightness temperature of the emitted synchrotron radiation signals at the frequencies 45 MHz and 408 MHz as a function of the galactic latitude $[-90^\circ, 90^\circ]$. The galactic longitude is set to $l = 0^\circ$. The WIMP primary annihilation channel is $\chi\chi \rightarrow b\bar{b}$, $M_{PBH} = 1M_\odot$. The PBH DM fraction f_{PBH} is varied for illustration. The observed radio emission data are also shown for comparison.

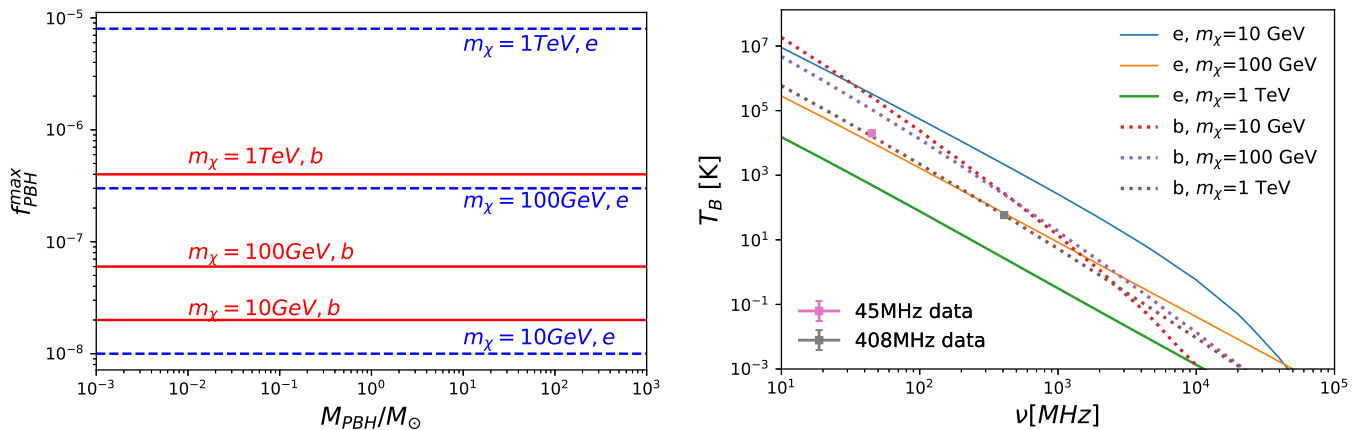


FIG. 3: [Left] The upper bounds for the allowed PBH DM fraction. The chosen WIMP annihilation channels are $\chi\chi \rightarrow b\bar{b}$ and $\chi\chi \rightarrow e^+e^-$ (e.g. $m_\chi = 100$ GeV, b means it is for $\chi\chi \rightarrow b\bar{b}$ with the WIMP mass 100 GeV). [Right] The brightness temperature of the synchrotron radiation as a function of the frequency at the Galactic center $((l, b) = (0^\circ, 0^\circ))$. The WIMP primary annihilation channels of $\chi\chi \rightarrow b\bar{b}$ and $\chi\chi \rightarrow e^+e^-$ are shown for comparison. $f_{PBH} = 10^{-7}$ is chosen for illustrative purposes. The error bars for the observation data points are too small to be seen in this figure.

is illustrated in the right panel of Fig. 3. The hadronic channel $\chi\chi \rightarrow b\bar{b}$ tends to have softer e^\pm energy spectrum than the leptonic channel $\chi\chi \rightarrow e^+e^-$ due to the hadronization. Consequently, $b\bar{b}$ annihilation scenario is more tightly constrained by the 45 MHz data than by 408 MHz data while the upper bound on f_{PBH} for e^+e^- annihilation scenario comes from 408 MHz data rather than from 45 MHz data for the electroweak scale WIMP mass range of our interest. Our synchrotron radio emission bounds turned out to be an order of magnitude less tight than those from the gamma ray and CMB bounds [18–21, 28, 30]. Our synchrotron radiation bounds nevertheless give the independent support for the claim that PBH DM and WIMP DM cannot coexist. We limited our analysis to 45 MHz and 408 MHz data sets for their large sky coverage and we found the bounds on f_{PBH} can change by a factor a few between these data sets for a given annihilation channel. Further improvement on the bounds could well be achievable by using the other data sets at the frequencies optimized to the specific DM annihilation models. The more systematic studies using larger radio observation data sets and more concrete particle physics models are left for future work.

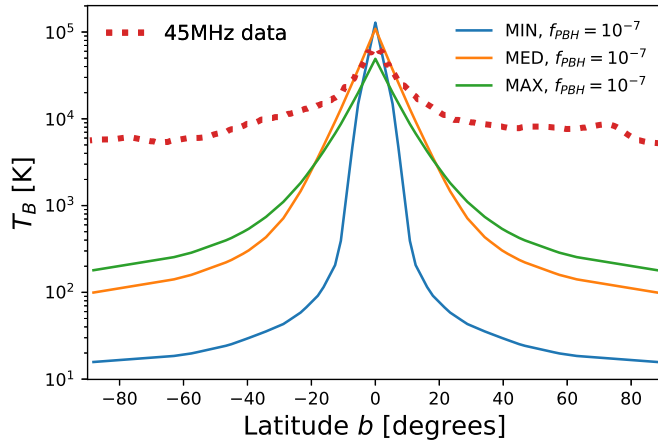


FIG. 4: The brightness temperature as a function of the galactic latitude $[-90^\circ, 90^\circ]$ at 45 MHz. The galactic longitude is set to $l = 0^\circ$. The WIMP primary annihilation channel is $\chi\chi \rightarrow b\bar{b}$, $M_{PBH} = 1M_\odot$, $m_\chi = 100$ GeV. The cosmic ray propagation parameters are varied among the MIN, MED, MAX models for comparison. $f_{PBH} = 10^{-7}$ is chosen for illustrative purposes.

IV. DISCUSSION/CONCLUSION

The synchrotron radiation predictions involve theoretical uncertainties such as those in the cosmic ray propagation model and magnetic field profile in Galaxy. Before concluding our discussions, let us briefly discuss how the predicted signals can be affected by these model uncertainties. The widely used propagation models in the literature are so-called MIN, MED, MAX models as mentioned in the last section, and we adopted the commonly used MED model in the last section. Fig. 4 shows the signals using the MIN and MAX model parameters for comparison. The radiation from the MIN model is confined to the Galactic center region while the MAX model has the thicker diffusive halo and the radiating e^\pm propagation extends to a larger region. While the signal predictions are indeed affected by the theoretical model uncertainties, the changes are within an order of magnitude among these conventional models and our bounds on f_{PBH} consequently would not change by more than an order of magnitude. We also varied the magnetic field profiles among MF1, MF2 and MF3 mentioned in the last section, and the difference in the brightness temperature is at most a factor a few and they give smaller effects on T_B than the propagation model variations shown in this figure. Hence we conclude that, even though the quantitative discussions can change due to the systematics in the theoretical modeling of cosmic ray propagation, the non-coexistence of PBH DM and WIMP DM is robust.

As commonly discussed in the literature discussing the UCMHs around PBHs, our tight bounds depend on the assumption that the kinetic energy of WIMPs is negligible in their forming the halos around PBHs. Accordingly we limited the values of M_{PBH}, m_χ to the range where the WIMP kinetic energy is of order a percent or less compared with the potential energy [18–21, 44, 47]. If the kinetic energy can interfere the gravitational influence of PBH on the WIMPs, the WIMP halos around PBHs can be less steep and hence the consequent annihilation signals will be reduced [18, 21, 44]. Such scenarios where the kinetic energy cannot be negligible is heavily dependent on the particle physics model assumptions such as the nature of WIMP kinetic decoupling from the thermal plasma in the early Universe, and such scenarios in view of the radio signals are left for future work. We focused on the signals from the Milky Way Galaxy in this paper and we plan to study the extra-galactic signals including the future prospects from the forthcoming radio experiments such as the SKA in our future work.

KK thanks P. Gondolo for the useful discussions. This work was partially supported by Grants-in-Aid for Scientific Research from JSPS (21K03533, 21H05459).

-
- [1] G. Jungman, M. Kamionkowski, and K. Griest, Supersymmetric dark matter, Phys. Rept. **267**, 195 (1996), arXiv:hep-ph/9506380.
 - [2] G. Bertone, D. Hooper, and J. Silk, Particle dark matter: Evidence, candidates and constraints, Phys. Rept. **405**, 279 (2005), arXiv:hep-ph/0404175.

- [3] R. D. Peccei and H. R. Quinn, CP Conservation in the Presence of Instantons, *Phys. Rev. Lett.* **38**, 1440 (1977), [328(1977)].
- [4] S. Weinberg, A New Light Boson?, *Phys. Rev. Lett.* **40**, 223 (1978).
- [5] F. Wilczek, Problem of Strong P and T Invariance in the Presence of Instantons, *Phys. Rev. Lett.* **40**, 279 (1978).
- [6] J. Preskill, M. B. Wise, and F. Wilczek, Cosmology of the Invisible Axion, *Phys. Lett. B* **120**, 127 (1983).
- [7] L. Abbott and P. Sikivie, A Cosmological Bound on the Invisible Axion, *Phys. Lett. B* **120**, 133 (1983).
- [8] M. Dine and W. Fischler, The Not So Harmless Axion, *Phys. Lett. B* **120**, 137 (1983).
- [9] B. P. Abbott et al. (LIGO Scientific, Virgo), Observation of Gravitational Waves from a Binary Black Hole Merger, *Phys. Rev. Lett.* **116**, 061102 (2016), arXiv:1602.03837 [gr-qc].
- [10] B. P. Abbott et al. (LIGO Scientific, Virgo), Binary Black Hole Mergers in the first Advanced LIGO Observing Run, *Phys. Rev. X* **6**, 041015 (2016), [Erratum: *Phys. Rev. X* **8**, 039903 (2018)], arXiv:1606.04856 [gr-qc].
- [11] B. P. Abbott et al. (LIGO Scientific, Virgo), Binary Black Hole Population Properties Inferred from the First and Second Observing Runs of Advanced LIGO and Advanced Virgo, *Astrophys. J. Lett.* **882**, L24 (2019), arXiv:1811.12940 [astro-ph.HE].
- [12] B. Carr and F. Kuhnel, Primordial Black Holes as Dark Matter: Recent Developments, (2020), arXiv:2006.02838 [astro-ph.CO].
- [13] A. M. Green and B. J. Kavanagh, Primordial Black Holes as a dark matter candidate, (2020), arXiv:2007.10722 [astro-ph.CO].
- [14] B. Carr, K. Kohri, Y. Sendouda, and J. Yokoyama, Constraints on Primordial Black Holes, (2020), arXiv:2002.12778 [astro-ph.CO].
- [15] P. Scott and S. Sivertsson, Gamma-Rays from Ultracompact Primordial Dark Matter Minihalos, *Phys. Rev. Lett.* **103**, 211301 (2009), [Erratum: *Phys. Rev. Lett.* **105**, 119902 (2010)], arXiv:0908.4082 [astro-ph.CO].
- [16] P. Gondolo and J. Silk, Dark matter annihilation at the galactic center, *Phys. Rev. Lett.* **83**, 1719 (1999), arXiv:astro-ph/9906391.
- [17] B. C. Lacki and J. F. Beacom, Primordial Black Holes as Dark Matter: Almost All or Almost Nothing, *Astrophys. J. Lett.* **720**, L67 (2010), arXiv:1003.3466 [astro-ph.CO].
- [18] S. M. Boucenna, F. Kuhnel, T. Ohlsson, and L. Visinelli, Novel Constraints on Mixed Dark-Matter Scenarios of Primordial Black Holes and WIMPs, *JCAP* **07**, 003, arXiv:1712.06383 [hep-ph].
- [19] J. Adamek, C. T. Byrnes, M. Gosenca, and S. Hotchkiss, WIMPs and stellar-mass primordial black holes are incompatible, *Phys. Rev. D* **100**, 023506 (2019), arXiv:1901.08528 [astro-ph.CO].
- [20] Y. Eroshenko, Dark matter density spikes around primordial black holes, *Astron. Lett.* **42**, 347 (2016), arXiv:1607.00612 [astro-ph.HE].
- [21] B. Carr, F. Kuhnel, and L. Visinelli, Black holes and WIMPs: all or nothing or something else, *Mon. Not. Roy. Astron. Soc.* **506**, 3648 (2021), arXiv:2011.01930 [astro-ph.CO].
- [22] R.-G. Cai, X.-Y. Yang, and Y.-F. Zhou, Constraints on mixed dark matter model of particles and primordial black holes from the Galactic 511 keV line, (2020), arXiv:2007.11804 [astro-ph.CO].
- [23] M. S. Delos, A. L. Erickcek, A. P. Bailey, and M. A. Alvarez, Density profiles of ultracompact minihalos: Implications for constraining the primordial power spectrum, *Phys. Rev. D* **98**, 063527 (2018), arXiv:1806.07389 [astro-ph.CO].
- [24] K. Kohri, T. Nakama, and T. Suyama, Testing scenarios of primordial black holes being the seeds of supermassive black holes by ultracompact minihalos and CMB μ -distortions, *Phys. Rev. D* **90**, 083514 (2014), arXiv:1405.5999 [astro-ph.CO].
- [25] G. Bertone, A. M. Coogan, D. Gaggero, B. J. Kavanagh, and C. Weniger, Primordial Black Holes as Silver Bullets for New Physics at the Weak Scale, *Phys. Rev. D* **100**, 123013 (2019), arXiv:1905.01238 [hep-ph].
- [26] S. Ando and K. Ishiwata, Constraints on decaying dark matter from the extragalactic gamma-ray background, *JCAP* **05**, 024, arXiv:1502.02007 [astro-ph.CO].
- [27] M. P. Hertzberg, S. Nurmi, E. D. Schiappacasse, and T. T. Yanagida, Shining Primordial Black Holes, (2020), arXiv:2011.05922 [hep-ph].
- [28] Y. Yang, The abundance of primordial black holes from the global 21cm signal and extragalactic gamma-ray background, *Eur. Phys. J. Plus* **135**, 690 (2020), arXiv:2008.11859 [astro-ph.CO].
- [29] D. Zhang, Impact of Primordial Ultracompact Minihaloes on the Intergalactic Medium and First Structure Formation, *Mon. Not. Roy. Astron. Soc.* **418**, 1850 (2011), arXiv:1011.1935 [astro-ph.CO].
- [30] H. Tashiro and K. Kadota, Constraining Mixed Dark-Matter Scenarios of WIMPs and Primordial Black Holes from CMB and 21-cm observations, *Phys. Rev. D* **103**, 123532 (2021), arXiv:2104.09738 [astro-ph.CO].
- [31] M. Cirelli and M. Taoso, Updated galactic radio constraints on Dark Matter, *JCAP* **07**, 041, arXiv:1604.06267 [hep-ph].
- [32] Y. Mambrini, M. H. G. Tytgat, G. Zaharijas, and B. Zaldivar, Complementarity of Galactic radio and collider data in constraining WIMP dark matter models, *JCAP* **11**, 038, arXiv:1206.2352 [hep-ph].
- [33] E. Borriello, A. Cuoco, and G. Miele, Radio constraints on dark matter annihilation in the galactic halo and its substructures, *Phys. Rev. D* **79**, 023518 (2009), arXiv:0809.2990 [astro-ph].
- [34] E. Storm, T. E. Jeltema, M. Spletstoesser, and S. Profumo, Synchrotron Emission from Dark Matter Annihilation: Predictions for Constraints from Non-detections of Galaxy Clusters with New Radio Surveys, *Astrophys. J.* **839**, 33 (2017), arXiv:1607.01049 [astro-ph.CO].
- [35] S. Colafrancesco, S. Profumo, and P. Ullio, Detecting dark matter WIMPs in the Draco dwarf: A multi-wavelength perspective, *Phys. Rev. D* **75**, 023513 (2007), arXiv:astro-ph/0607073.
- [36] G. Bertone, M. Cirelli, A. Strumia, and M. Taoso, Gamma-ray and radio tests of the $e+e-$ excess from DM annihilations, *JCAP* **03**, 009, arXiv:0811.3744 [astro-ph].

- [37] M. Regis and P. Ullio, Multi-wavelength signals of dark matter annihilations at the Galactic center, *Phys. Rev. D* **78**, 043505 (2008), arXiv:0802.0234 [hep-ph].
- [38] A. Paul, D. Majumdar, and A. Dutta Banik, Signatures of synchrotron radiation from the annihilation of dark matter at the Galactic Centre, *JCAP* **05**, 029, arXiv:1812.10791 [hep-ph].
- [39] B. Dutta, A. Kar, and L. E. Strigari, Constraints on MeV dark matter and primordial black holes: Inverse Compton signals at the SKA, *JCAP* **03**, 011, arXiv:2010.05977 [astro-ph.HE].
- [40] S. Mittal and G. Kulkarni, Background of radio photons from primordial black holes 10.1093/mnras/stac005 (2021), arXiv:2110.11975 [astro-ph.CO].
- [41] H. Poulter, Y. Ali-Haïmoud, J. Hamann, M. White, and A. G. Williams, CMB constraints on ultra-light primordial black holes with extended mass distributions, (2019), arXiv:1907.06485 [astro-ph.CO].
- [42] U. Mukhopadhyay, D. Majumdar, and A. Paul, Discriminating and Constraining the Synchrotron and Inverse Compton Radiations from Primordial Black Hole and Dark Matter at the Galactic Centre Region, (2021), arXiv:2109.14955 [astro-ph.CO].
- [43] M. H. Chan and C. M. Lee, Constraining Primordial Black Hole Fraction at the Galactic Centre using radio observational data, *Mon. Not. Roy. Astron. Soc.* **497**, 1212 (2020), arXiv:2007.05677 [astro-ph.HE].
- [44] M. Boudaud, T. Lacroix, M. Stref, J. Lavalle, and P. Salati, In-depth analysis of the clustering of dark matter particles around primordial black holes. Part I. Density profiles, *JCAP* **08**, 053, arXiv:2106.07480 [astro-ph.CO].
- [45] N. Afshordi, P. McDonald, and D. Spergel, Primordial black holes as dark matter: The Power spectrum and evaporation of early structures, *Astrophys. J. Lett.* **594**, L71 (2003), arXiv:astro-ph/0302035.
- [46] H. Tashiro and K. Kadota, CMB and 21-cm bounds on early structure formation boosted by primordial black hole entropy fluctuations, *Phys. Rev. D* **104**, 063522 (2021), arXiv:2105.08462 [astro-ph.CO].
- [47] K. Kadota and J. Silk, Boosting small-scale structure via primordial black holes and implications for sub-GeV dark matter annihilation, *Phys. Rev. D* **103**, 043530 (2021), arXiv:2012.03698 [astro-ph.CO].
- [48] D. Inman and Y. Ali-Haïmoud, Early structure formation in primordial black hole cosmologies, *Phys. Rev. D* **100**, 083528 (2019), arXiv:1907.08129 [astro-ph.CO].
- [49] R. Murgia, G. Scelfo, M. Viel, and A. Raccanelli, Lyman- α Forest Constraints on Primordial Black Holes as Dark Matter, *Phys. Rev. Lett.* **123**, 071102 (2019), arXiv:1903.10509 [astro-ph.CO].
- [50] M. Oguri and R. Takahashi, Probing Dark Low Mass Halos and Primordial Black Holes with Frequency Dependent Gravitational Lensing Dispersions of Gravitational Waves, (2020), arXiv:2007.01936 [astro-ph.CO].
- [51] J.-O. Gong and N. Kitajima, Small-scale structure and 21cm fluctuations by primordial black holes, *JCAP* **08**, 017, arXiv:1704.04132 [astro-ph.CO].
- [52] B. Carr and J. Silk, Primordial Black Holes as Generators of Cosmic Structures, *Mon. Not. Roy. Astron. Soc.* **478**, 3756 (2018), arXiv:1801.00672 [astro-ph.CO].
- [53] O. Mena, S. Palomares-Ruiz, P. Villanueva-Domingo, and S. J. Witte, Constraining the primordial black hole abundance with 21-cm cosmology, *Phys. Rev. D* **100**, 043540 (2019), arXiv:1906.07735 [astro-ph.CO].
- [54] A. Loeb and M. Zaldarriaga, The Small-scale power spectrum of cold dark matter, *Phys. Rev. D* **71**, 103520 (2005), arXiv:astro-ph/0504112.
- [55] E. Bertschinger, The Effects of Cold Dark Matter Decoupling and Pair Annihilation on Cosmological Perturbations, *Phys. Rev. D* **74**, 063509 (2006), arXiv:astro-ph/0607319.
- [56] P. Gondolo, J. Hisano, and K. Kadota, The Effect of quark interactions on dark matter kinetic decoupling and the mass of the smallest dark halos, *Phys. Rev. D* **86**, 083523 (2012), arXiv:1205.1914 [hep-ph].
- [57] S. Profumo, K. Sigurdson, and M. Kamionkowski, What mass are the smallest protohalos?, *Phys. Rev. Lett.* **97**, 031301 (2006), arXiv:astro-ph/0603373.
- [58] P. Gondolo and K. Kadota, Late Kinetic Decoupling of Light Magnetic Dipole Dark Matter, *JCAP* **06**, 012, arXiv:1603.05783 [hep-ph].
- [59] A. M. Green, S. Hofmann, and D. J. Schwarz, The power spectrum of SUSY - CDM on sub-galactic scales, *Mon. Not. Roy. Astron. Soc.* **353**, L23 (2004), arXiv:astro-ph/0309621.
- [60] A. M. Green, S. Hofmann, and D. J. Schwarz, The First wimpy halos, *JCAP* **08**, 003, arXiv:astro-ph/0503387.
- [61] T. Bringmann and S. Hofmann, Thermal decoupling of WIMPs from first principles, *JCAP* **04**, 016, [Erratum: *JCAP* **03**, E02 (2016)], arXiv:hep-ph/0612238.
- [62] P. D. Serpico, V. Poulin, D. Inman, and K. Kohri, Cosmic microwave background bounds on primordial black holes including dark matter halo accretion, *Phys. Rev. Res.* **2**, 023204 (2020), arXiv:2002.10771 [astro-ph.CO].
- [63] J. F. Navarro, C. S. Frenk, and S. D. M. White, The Structure of cold dark matter halos, *Astrophys. J.* **462**, 563 (1996), arXiv:astro-ph/9508025.
- [64] J. Shelton, S. L. Shapiro, and B. D. Fields, Black hole window into p -wave dark matter annihilation, *Phys. Rev. Lett.* **115**, 231302 (2015), arXiv:1506.04143 [astro-ph.HE].
- [65] B. D. Fields, S. L. Shapiro, and J. Shelton, Galactic Center Gamma-Ray Excess from Dark Matter Annihilation: Is There A Black Hole Spike?, *Phys. Rev. Lett.* **113**, 151302 (2014), arXiv:1406.4856 [astro-ph.HE].
- [66] S. L. Shapiro and J. Shelton, Weak annihilation cusp inside the dark matter spike about a black hole, *Phys. Rev. D* **93**, 123510 (2016), arXiv:1606.01248 [astro-ph.HE].
- [67] C. Johnson, R. Caputo, C. Karwin, S. Murgia, S. Ritz, and J. Shelton, Search for gamma-ray emission from p -wave dark matter annihilation in the Galactic Center, *Phys. Rev. D* **99**, 103007 (2019), arXiv:1904.06261 [astro-ph.HE].
- [68] P. Ullio, H. Zhao, and M. Kamionkowski, A Dark matter spike at the galactic center?, *Phys. Rev. D* **64**, 043504 (2001), arXiv:astro-ph/0101481.

- [69] E. Vasiliev, Dark matter annihilation near a black hole: Plateau vs. weak cusp, *Phys. Rev. D* **76**, 103532 (2007), arXiv:0707.3334 [astro-ph].
- [70] L. Sadeghian, F. Ferrer, and C. M. Will, Dark matter distributions around massive black holes: A general relativistic analysis, *Phys. Rev. D* **88**, 063522 (2013), arXiv:1305.2619 [astro-ph.GA].
- [71] K. Kadota and H. Tashiro, Primordial black hole dark matter in the presence of p-wave WIMP annihilation, *JCAP* **03** (03), 045, arXiv:2112.04179 [astro-ph.CO].
- [72] M. S. Longair, *High Energy Astrophysics* (Cambridge University Press, 2011).
- [73] E. A. Baltz and J. Edsjo, Positron propagation and fluxes from neutralino annihilation in the halo, *Phys. Rev. D* **59**, 023511 (1998), arXiv:astro-ph/9808243.
- [74] T. Delahaye, R. Lineros, F. Donato, N. Fornengo, and P. Salati, Positrons from dark matter annihilation in the galactic halo: Theoretical uncertainties, *Phys. Rev. D* **77**, 063527 (2008), arXiv:0712.2312 [astro-ph].
- [75] S. Colafrancesco, S. Profumo, and P. Ullio, Multi-frequency analysis of neutralino dark matter annihilations in the Coma cluster, *Astron. Astrophys.* **455**, 21 (2006), arXiv:astro-ph/0507575.
- [76] D. Hooper, A. V. Belikov, T. E. Jeltema, T. Linden, S. Profumo, and T. R. Slatyer, The Isotropic Radio Background and Annihilating Dark Matter, *Phys. Rev. D* **86**, 103003 (2012), arXiv:1203.3547 [astro-ph.CO].
- [77] A. McDaniel, T. Jeltema, S. Profumo, and E. Storm, Multiwavelength Analysis of Dark Matter Annihilation and RX-DMFIT, *JCAP* **09**, 027, arXiv:1705.09384 [astro-ph.HE].
- [78] N. Fornengo, R. A. Lineros, M. Regis, and M. Taoso, Galactic synchrotron emission from WIMPs at radio frequencies, *JCAP* **01**, 005, arXiv:1110.4337 [astro-ph.GA].
- [79] J. Buch, M. Cirelli, G. Giesen, and M. Taoso, PPPC 4 DM secondary: A Poor Particle Physicist Cookbook for secondary radiation from Dark Matter, *JCAP* **09**, 037, arXiv:1505.01049 [hep-ph].
- [80] M. Cirelli, P. D. Serpico, and G. Zaharijas, Bremsstrahlung gamma rays from light Dark Matter, *JCAP* **11**, 035, arXiv:1307.7152 [astro-ph.HE].
- [81] R. Saito and S. Shirai, Primordial Black Hole as a Source of the Boost Factor, *Phys. Lett. B* **697**, 95 (2011), arXiv:1009.1947 [hep-ph].
- [82] T. Goerdt, O. Y. Gnedin, B. Moore, J. Diemand, and J. Stadel, The survival and disruption of CDM microhaloes: Implications for direct and indirect detection experiments, *Mon. Not. Roy. Astron. Soc.* **375**, 191 (2007), arXiv:astro-ph/0608495.
- [83] F. C. van den Bosch, G. Ogiya, O. Hahn, and A. Burkert, Disruption of Dark Matter Substructure: Fact or Fiction?, *Mon. Not. Roy. Astron. Soc.* **474**, 3043 (2018), arXiv:1711.05276 [astro-ph.GA].
- [84] L. Xie and L. Gao, Assembly history of subhalo populations in galactic and cluster sized dark haloes, *MNRAS* **454**, 1697 (2015), arXiv:1501.03171 [astro-ph.CO].
- [85] V. Berezhinsky, V. Dokuchaev, and Y. Eroshenko, Remnants of dark matter clumps, *Phys. Rev. D* **77**, 083519 (2008), arXiv:0712.3499 [astro-ph].
- [86] M. S. Delos, Tidal evolution of dark matter annihilation rates in subhalos, *Phys. Rev. D* **100**, 063505 (2019), arXiv:1906.10690 [astro-ph.CO].
- [87] S. B. Green and F. C. van den Bosch, The tidal evolution of dark matter substructure – I. subhalo density profiles, *Mon. Not. Roy. Astron. Soc.* **490**, 2091 (2019), arXiv:1908.08537 [astro-ph.GA].
- [88] V. Berezhinsky, V. Dokuchaev, Y. Eroshenko, M. Kachelrieß, and M. A. Solberg, Superdense cosmological dark matter clumps, *Phys. Rev. D* **81**, 103529 (2010), arXiv:1002.3444 [astro-ph.CO].
- [89] A. M. Green and S. P. Goodwin, On mini-halo encounters with stars, *Mon. Not. Roy. Astron. Soc.* **375**, 1111 (2007), arXiv:astro-ph/0604142.
- [90] A. Schneider, L. Krauss, and B. Moore, Impact of Dark Matter Microhalos on Signatures for Direct and Indirect Detection, *Phys. Rev. D* **82**, 063525 (2010), arXiv:1004.5432 [astro-ph.GA].
- [91] M. Cirelli, G. Corcella, A. Hektor, G. Hutsi, M. Kadastik, P. Panci, M. Raidal, F. Sala, and A. Strumia, PPPC 4 DM ID: A Poor Particle Physicist Cookbook for Dark Matter Indirect Detection, *JCAP* **03**, 051, [Erratum: *JCAP* **10**, E01 (2012)], arXiv:1012.4515 [hep-ph].
- [92] F. Donato, N. Fornengo, D. Maurin, and P. Salati, Antiprotons in cosmic rays from neutralino annihilation, *Phys. Rev. D* **69**, 063501 (2004), arXiv:astro-ph/0306207.
- [93] K. Blum, Cosmic ray propagation time scales: lessons from radioactive nuclei and positron data, *JCAP* **11**, 037, arXiv:1010.2836 [astro-ph.HE].
- [94] A. W. Strong, I. V. Moskalenko, and O. Reimer, Diffuse continuum gamma-rays from the galaxy, *Astrophys. J.* **537**, 763 (2000), [Erratum: *Astrophys. J.* **541**, 1109 (2000)], arXiv:astro-ph/9811296.
- [95] X. H. Sun, W. Reich, A. Waelkens, and T. Enslin, Radio observational constraints on Galactic 3D-emission models, *Astron. Astrophys.* **477**, 573 (2008), arXiv:0711.1572 [astro-ph].
- [96] A. W. Strong, E. Orlando, and T. R. Jaffe, The interstellar cosmic-ray electron spectrum from synchrotron radiation and direct measurements, *Astron. Astrophys.* **534**, A54 (2011), arXiv:1108.4822 [astro-ph.HE].
- [97] A. E. Vladimirov, S. W. Digel, G. Johannesson, P. F. Michelson, I. V. Moskalenko, P. L. Nolan, E. Orlando, T. A. Porter, and A. W. Strong, GALPROP WebRun: an internet-based service for calculating galactic cosmic ray propagation and associated photon emissions, *Comput. Phys. Commun.* **182**, 1156 (2011), arXiv:1008.3642 [astro-ph.HE].
- [98] A. E. Guzman, J. May, H. Alvarez, and K. Maeda, All-sky Galactic radiation at 45 MHz and spectral index between 45 and 408 MHz, *Astron. Astrophys.* **525**, A138 (2011), arXiv:1011.4298 [astro-ph.GA].
- [99] Planck legacy archive, <https://wiki.cosmos.esa.int/planck-legacy-archive/>.
- [100] N. Fornengo, R. A. Lineros, M. Regis, and M. Taoso, The isotropic radio background revisited, *JCAP* **04**, 008,

arXiv:1402.2218 [astro-ph.CO].

- [101] R. Adam et al. (Planck), Planck intermediate results.: XLII. Large-scale Galactic magnetic fields, *Astron. Astrophys.* **596**, A103 (2016), arXiv:1601.00546 [astro-ph.GA].